

First-principles investigations for YH_3 (YD_3): Energetics, electric-field gradients, and optical properties

W. Wolf

Materials Design s. a. r. l., 44, av. F.-A. Bartholdi, 72000 Le Mans, France

P. Herzig

Institut für Physikalische Chemie, Universität Wien, Währinger Straße 42, 1090 Vienna, Austria

(Received 9 July 2002; published 20 December 2002)

The crystallographic structure of switchable mirror material YD_3 is still under debate. Aiming at a final structure assessment, currently considered structure models of $P\bar{3}c1$, $P6_3cm$ and $P6_3$ symmetry are studied by means of *ab initio* methods. The relative stability of these candidate structures is investigated by a comparison of total energies, where the structural parameters are derived from experiments, and in addition are calculated by geometry optimization. The $P6_3$ structure is found to yield the lowest energy, followed, in this order, by the $P6_3cm$ and $P\bar{3}c1$ structures. The energy differences between these structures, however, are as small as 0.01 eV per unit cell of six formula units and are thus too small for definitive structure assignments. In addition, electric-field gradients for the D and Y atoms were calculated for the three structures applying the optimized structural parameters, and are compared to experimental data obtained recently by deuteron magnetic resonance for $\text{YD}_{2,98}$ as well as substitutions for the Y nucleus. Best agreement is observed for the structure with $P6_3cm$ symmetry. For the $P6_3cm$ structure we also calculated the band structure and the optical transitions on the basis of the screened-exchange local-density approximation, and obtained a medium-band-gap semiconductor. The relative position of valence and conduction band edge states as well as other states close to the Fermi level seem to be in agreement with available experimental data.

DOI: 10.1103/PhysRevB.66.224112

PACS number(s): 81.05.Je, 76.60.Gv, 71.15.Mb, 71.15.Nc

I. INTRODUCTION

Since the important discovery in 1996 by Huiberts *et al.*¹ that yttrium and lanthanum hydride films have switchable optical properties at ambient temperatures, these hydrides have attracted much interest, although the underlying reversible metal-insulator transitions for stoichiometries close to three H atoms per metal atom² have been known for quite some time.³⁻⁵ For a Y-H system there are three well-defined phases at room temperature. Particularly for the trihydride phase a large number of experimental and theoretical investigations have been carried out. However, a final answer to the question about the exact crystal structure of the compound YH_3 can still not be provided. A first neutron powder diffraction study⁶ 30 years ago assigned to YH_3 (Ref. 7) the ideal HoD_3 structure with its $P\bar{3}c1$ symmetry. This structure is derived from the LiF_3 structure where all non-metal atoms at octahedral sites lie exactly in the planes of the metal atoms. In the ideal HoD_3 structure two-thirds of the octahedral H atoms are shifted slightly above and below the metal planes. Later Udovic *et al.*⁸ found, from neutron-powder-diffraction experiments, an unusual displacement of the hydrogen atoms from their ideal positions. The greater stability of the latter structure was confirmed by total energy calculations based on first principles.⁹ Recently Udovic and co-workers^{10,11} also assumed a noncentrosymmetric structure with $P6_3cm$ symmetry to be compatible to their neutron-diffraction data. Apart from these structure models provided by the experimentalists a further proposal came from *ab initio* molecular dynamics calculations by Kelly *et al.*¹² for a structure with space group $P6_3$ (originally given as $P3$).

The latter structure is energetically more favorable than the $P\bar{3}c1$ structure and also leads to a band gap even within the local-density approximation (LDA), but seems to contradict the neutron-diffraction results.^{13,14} In structures with $P6_3cm$ and $P6_3$ symmetry all octahedral H atoms are shifted out of the metal plane although their arrangement is different.^{11,15} In the following the structure symbols I and II refer to two different, correspondingly designated structural models by Udovic *et al.*⁸ with $P\bar{3}c1$ symmetry, while the structures with $P6_3cm$ and $P6_3$ symmetry are denoted as structures III and IV, respectively.

In order to solve the structure problem a few approaches have so far been chosen. Kierey *et al.*¹⁶ investigated the first-order Raman spectra of YH_3 and YD_3 . The number of A_1 modes observed by these authors is not compatible with a $P\bar{3}c1$ structure, but their findings seem to be in agreement with the noncentrosymmetric $P6_3cm$ and $P6_3$ structures. In another approach van Gelderen *et al.*¹⁵ calculated phonon densities of states for the $P\bar{3}c1$ structure and the broken symmetry ($P6_3$) structure, and compared them to results from neutron vibration spectroscopy. These authors found a significantly worse agreement for the $P\bar{3}c1$ structure than for the broken symmetry structure. Furthermore, Herzig *et al.*¹⁷ and Żogał *et al.*¹⁸ used the electric-field gradients (EFG's) for D in YD_3 to draw conclusions about possible structure models by comparing the experimental results with results calculated for the $P\bar{3}c1$ and $P6_3cm$ structures. It turned out that a better agreement is found for the latter of the two structures in accordance with Kierey *et al.*¹⁶

The purpose of the present paper is to provide further

material for a final structure assessment for YH_3 . The phase stabilities of the three candidate structures are explored by total-energy calculations based on structural parameters as characterized experimentally and as calculated by minimization of atomic forces and stress tensors. An efficient and accurate projector augmented wave scheme was chosen as the most suitable for this task. Moreover, EFG's have been calculated for all the candidate structures with structural parameters optimized by the previous step. In order to satisfy the very high accuracy requirements for the treatment of all electrons of the system necessary to obtain reliable EFG's, an all-electron full-potential augmented plane wave approach was pursued for this task. Finally, the semiconducting nature of the $P6_3cm$ structure of YH_3 is demonstrated. The band gap and possible optical transitions are calculated by the all-electron full-potential method enhanced by the screened-exchange local-density approximation (sX-LDA),^{19,20} in order to overcome the inability of standard density-functional theory to accurately predict excitation energies.

II. COMPUTATIONAL DETAILS

A. Projector augmented wave structure optimization and total-energy calculations

An optimization of structural parameters and calculation of total energies was performed by the Vienna *ab initio* simulation package (VASP).^{21–23} VASP solves the Kohn-Sham equations of density-functional theory^{24,25} with periodic boundary conditions by an iterative diagonalization. We employed a conjugate gradient technique for the diagonalization, and projection operators were accurately evaluated in reciprocal space. The method is based on plane waves and the electron-ion interaction is described either by means of the projector augmented wave (PAW) method^{26,27} or ultrasoft pseudopotentials²⁸ (USP's). The yttrium PAW potential includes $4s4p5s4d$, whereas USP's consider the $4p5s4d$ configuration as valence states. Most of our study is based on the rigorous and accurate PAW scheme, but the USP scheme has also been applied for some cases to enable comparison. Exchange and correlation are treated within the LDA in the functional form given by Perdew and Zunger.²⁹ In addition, nonlocal corrections are taken into account by the generalized gradient approximation (GGA) of Perdew *et al.*³⁰ Reciprocal space sampling was performed using $7 \times 7 \times 7$ Monkhorst-Pack³¹ meshes and reciprocal-space integration has been performed by the linear tetrahedron method^{32,33} including the Blöchl correction.³⁴ Optimization of structural parameters was achieved by a minimization of atomic forces and stress tensors applying the conjugate gradient technique. For this task two levels of accuracy were chosen to test the convergence of the results of geometry optimization and total energies, i.e., a typical setup with a cutoff energy of 312.5 eV and a perfectly converged setup with a cutoff energy of about 1115 eV. For both cases, Fourier grids are chosen to be large enough to avoid wraparound errors.

B. All-electron EFG calculations

The all-electron calculations are based on the density-functional theory^{24,25} (DFT) and the local-density approxi-

mation, and have been performed by the linearized augmented plane-wave (LAPW) method³⁵ in its full-potential version^{36–39} (FLAPW) using an exchange-correlation potential by Hedin and Lundqvist.^{40,41}

The parameters in the FLAPW calculation have been chosen as follows and are the same for all YD_3 structures except where indicated explicitly. For the l expansion of the potential and the electron density inside the muffin-tin spheres terms up to $l=8$ were taken into account. In agreement with our previous calculations^{17,18} the muffin-tin radii for Y and D were set to 1.4027 and 0.7062 Å, respectively. Plane waves for the wave functions in the interstitial region were included up to a length of 4.0 in units of $2\pi/a$, a choice which corresponds to circa 1700 basis functions per unit cell (for six formula units of YD_3). While in our recent paper,¹⁸ for the $P\bar{3}c1$ and $P6_3cm$ structures, a $9 \times 9 \times 9$ Monkhorst and Pack³¹ mesh was employed in the self-consistency procedure for the valence states (corresponding to 88 and 60 \mathbf{k} points for the two structures), we now used a $7 \times 7 \times 7$ mesh in all cases (corresponding to 44, 32, and 36 \mathbf{k} points for the $P\bar{3}c1$, $P6_3cm$, and $P6_3$ structures, respectively). The higher-lying Y core states ($4s$ and $4p$) have been treated as band states in a second energy window for which we now used a $3 \times 3 \times 3$ Monkhorst and Pack mesh (corresponding to 7 \mathbf{k} points for the $P\bar{3}c1$ and 6 \mathbf{k} points for the $P6_3cm$ and $P6_3$ structures) instead of a $5 \times 5 \times 5$ mesh in our previous investigation. This reduction of the number of \mathbf{k} points is justified as was tested for the $P\bar{3}c1$ structure where no significant changes in the EFG results have been observed.

The reciprocal-space integration has been performed by the linear tetrahedron method^{32,33} including the Blöchl correction.³⁴ For maximum accuracy of the EFG's, the non-spherical terms of the matrix elements have been calculated for the full Hamiltonian without any approximation.

The EFG's have been calculated by taking the $l=2$ components of the Coulomb potential near the Y or D nuclei. The formalism by Herzig⁴² and Blaha *et al.*⁴³ has also been employed to split the calculated EFG components into the contributions from the surrounding electrons within the respective muffin-tin sphere ("sphere contribution") and the remainder that comes from outside this sphere ("lattice contribution"). This partitioning depends, to a small extent, on the choice of the muffin-tin radii. The valence contribution can be split further into sd , pp , dd , pf , and ff contributions which provide useful information about the influence of particular l -like wave functions on the EFG's.⁴⁴

In the following V_{zz} is the EFG component with the largest absolute value and V_{xx} the one with the smallest absolute value. Since the EFG is a traceless tensor the condition

$$V_{xx} + V_{yy} + V_{zz} = 0 \quad (1)$$

must hold. The asymmetry parameter η is defined as

$$\eta = \frac{V_{xx} - V_{yy}}{V_{zz}}. \quad (2)$$

TABLE I. Total energy per unit cell (6 formula units) in eV relative to the total energy of structure III.

Structure	Expt. structural parameters					Calc. structural parameters	
	LDA			GGA		GGA setup	
	FLAPW	PAW	USP	PAW	USP	Typical	Converged
I ($P\bar{3}c1$)	0.0169	0.0189	0.0187	0.0245	0.0238	0.0113	0.0095
II ($P\bar{3}c1$)	-0.0058	-0.0019	-0.0017	-0.0005	-0.0006	0.0123	0.0096
III ($P6_3cm$)	0.0	0.0	0.0	0.0	0.0	0.0	0.0
IV ($P6_3$)	-	-	-	-	-	-0.0095	-0.0119

C. Screened-exchange LDA band-gap calculations

Density-functional theory has proved to be very suitable for an accurate prediction of ground-state properties, such as equilibrium structural parameters, phase stabilities, elastic constants or electric-field gradients. However, excitation energies and band gaps of semiconductors and insulators are definitively beyond the scope of a theoretical concept designed for the ground state. Consequently, band gaps are typically obtained much too small by conventional DFT. In particular, DFT calculations of the band structure of the HoD_3 structure type of YH_3 yielded a semimetal with a large band overlap at the Γ point.^{9,47} In our study of the band gap and optical properties of semiconducting YH_3 of type III it is thus necessary to choose an approach beyond density-functional theory. To this end we apply a FLAPW implementation⁴⁸ of the screened-exchange local-density approximation (sX-LDA),^{19,20} which has proved to be very successful in predicting band gaps, band topology and effective masses of a wide range of semiconductors.⁴⁹

The sX-LDA concept is based on a separation of the exchange-correlation operator into two parts: a weakly wavefunction-dependent part is still approximated as a functional of the density within the LDA, whereas the remainder is treated exactly. The exact nonlocal Hartree-Fock exchange operator is evaluated with a screened Coulomb interaction. The screening is static, and local-field effects are not taken into account. Since the Thomas-Fermi wave vector of the screening term is calculated from the average density in the crystal, this approach does not rely on any empirical parameter.

For the calculations presented in this work the non-local screened exchange operator was built on a $3 \times 3 \times 3$ Monkhorst and Pack grid yielding 27 \mathbf{k} points in the full Brillouin zone. The sX-LDA wave functions were iteratively improved until self-consistency was reached. The screening cutoff could be reduced down to 2.5 in units of $2\pi/a$, reproducing eigenvalues within 0.05 eV. The band structure was calculated on a grid of 110 \mathbf{k} points along the chosen path through the Brillouin zone. Other computational parameters were chosen identical to those used for EFG calculations (see Sec. II B).

III. STRUCTURAL PARAMETERS AND TOTAL ENERGIES

The phase stability of the candidate structures is investigated based on comparison of total energies calculated by

VASP and the FLAPW approach. In a first step, structural parameters of types I–III were taken from experimental studies (structure IV has not been characterized experimentally) and the resulting total energies are compared in the left section of Table I for most relevant computational options. In fact, these options reflect the most important approximations that need to be imposed to obtain a computationally feasible approach. We compare the results for different approximations to exchange and correlation, i.e., LDA versus GGA, and the type of potential, i.e., USP versus PAW. It turns out that the results are quite insensitive to the choice of these approximations. Structure II is found to be the lowest in energy irrespective of the computational procedure. Structure III is almost as low in energy as structure II, and structure I is found to be of highest energy. This hierarchy is reproduced by any of the chosen computational options for VASP. As a further test the total energies of the three structures have also been calculated by the all-electron FLAPW method within the LDA reproducing the VASP results. For all of these computational options, relative energy differences between these structures are in the range of 0.0245 and 0.0005 eV per unit cell (six formula units) and are thus very small. Therefore, at room temperature all of these structures are accessible.

As a further step toward consistency, the structural parameters of all four structures were not taken from experiments but were calculated by atomic forces and stress tensor minimization. As mentioned in Sec. II A, two different energy cutoffs for the plane wave basis were applied, corresponding to a typical and a highly converged setup. As can be observed on the right hand side of Table I, where the relative total energies after geometry optimization are summarized, both levels of convergence yield a very similar ranking of structures, which is, however, different from that one obtained from the experimental structures. The broken symmetry structure IV is now lowest in total energy, but is followed by structures III and I/II. Structures I and II are of the same structure type with different structural parameters and thus should yield identical total energies after geometry optimization. The discrepancies of 0.001 and 0.0001 eV for both computational setups provide an estimate of the errors involved. Also after geometry optimization the differences in total energies are very small, and are thus only capable of providing indications for stability, but are not well suited for a definitive structure determination.

Table II compares the structural parameters as obtained from geometry optimization and from experimental studies.

TABLE II. Structural parameters obtained from experiments and from structure optimization. Lattice parameters a and c are given in Å.

Structure model	Parameter	Experimental	Optimized		
			Normal basis	Huge basis	
I	a	6.3442	6.3013	6.3408	
	c	6.5999	6.5567	6.6061	
	Y: $6f$	x	0.6665	0.6631	0.6628
	D(T): $12g$	x	0.3542	0.3502	0.3521
		y	0.0311	0.0283	0.0303
		z	0.0902	0.0923	0.0918
	D($m2$): $4d$	z	0.1874	0.1847	0.1875
	II	a	6.3440	6.3001	6.3409
c		6.5997	6.5569	6.6099	
Y: $6f$		x	0.6637	0.6631	0.6630
D(T): $12g$		x	0.3521	0.3505	0.3523
		y	0.0321	0.0287	0.0301
		z	0.0903	0.0922	0.0918
D($m2$): $4d$		z	0.1882	0.1853	0.1873
III		a	6.3441	6.2987	6.3441
	c	6.5998	6.5544	6.6117	
	Y: $6c$	x	0.6717	0.6699	0.6704
	D(1): $6c$	z	0.25	0.2507	0.2502
		x	0.3054	0.3039	0.3026
	D(2): $6c$	z	0.0898	0.0924	0.0915
		x	0.3601	0.3540	0.3556
	D(3): $2a$	z	0.4090	0.4081	0.4077
		z	0.3166	0.3191	0.3157
	D(4): $4b$	z	0.2073	0.2023	0.2068
IV	a		6.3017	6.3441	
	c		6.5517	6.6081	
	Y: $6c$	x		-0.3291	-0.3287
		y		-0.3320	-0.3322
		z		0.2505	0.2506
		x		-0.0178	-0.0183
	D(1): $6c$	y		-0.3647	-0.3667
		z		0.0924	0.0922
		x		0.3030	0.3017
	D(2): $6c$	y		-0.0040	-0.0042
		z		-0.0912	-0.0911
		z		0.1822	0.1870
	D(3): $2a$	z		0.2806	0.2788
D(4): $2b$	z		-0.1898	-0.1929	
D(5): $2b$	z				

Whereas typical deviations from experimental data are observed for the results of the typical setup, the converged setup yields outstandingly good agreement of all computed structural parameters with those from experiments. This may again serve as an indication that our computational approach is very well suited to tackle the problems under consideration.

The structural parameters obtained by the converged setup are now used for calculating EFG's for these compounds. In order to achieve the highest possible accuracy for the EFG

data, these calculations are performed by the FLAPW method. In contrast to the PAW method the FLAPW approach is a true all-electron method where core-electron states are also iteratively adapted to the crystal potential during the SCF procedure.

IV. ELECTRIC-FIELD GRADIENTS

The comparison of calculated and experimental EFG's is very suitable to exclude structure models for which there is a

disagreement in the EFG's. Therefore, the available experimental and theoretical information shall be reviewed and discussed with regard to the first-principles results reported in the present paper.

The following three experimental investigations have been performed up to now. Using ^{181}Ta -doped YH_3 in perturbed angular correlation measurements⁵⁰ the EFG at the Y site has been obtained. A direct EFG determination for Y is not possible because ^{89}Y , the only naturally occurring isotope, has a nuclear spin of $\frac{1}{2}$. NMR measurements for the D atoms in YD_3 have been performed by Balbach *et al.*⁵¹ and by Żogał *et al.*,¹⁸ although explicit EFG values are given only by the latter authors.⁶¹

Until now EFG calculations have only been performed for the D atoms in YD_3 (see Refs. 17 and 18). In the present study we give results also for the Y atoms. Furthermore, all EFG calculations refer to the optimized structural parameters, and thus consistent EFG data also become available for structure IV for which measured structural parameters are not available.

The EFG's for the relaxed structures I/II, III, and IV, together with the structural parameters used for the calculation, and the experimental EFG values for YD_3 , are presented in Table III. It should be noticed that for the experimental V_{zz} values the signs cannot be measured, and are therefore unknown. For the calculated results for the unrelaxed structures I, II, and III, see Ref. 18. As in our previous investigation agreement is best for structure III, although the structure relaxation shows that for the deuterium EFG's the asymmetry parameters are quite sensitive to small structural changes. The V_{zz} values are rather similar for all three structures. The calculated η values for D(*T*) and D(1) for structures I/II and IV, respectively, are too high.

Inspecting the Y EFG's, better agreement is found between the experimental value for V_{zz} (Ref. 50) and the calculated results for structure III and IV than for structure I/II. However, the results obtained from perturbed angular correlation measurements⁵⁰ studying the quadrupole interaction in ^{181}Hf -doped YH_3 have to be considered with care because of the probable trapping of hydrogen by the relatively high concentrations (0.5 at.%) of Hf and its daughter product Ta. New experiments might therefore be useful to obtain more reliable information.

Now the EFG results shall be discussed in more detail. This requires a splitting of the sphere contribution to the calculated EFG's into ll' -like contributions. Since the Cartesian components of the EFG tensor are normally given with respect to its principal axes, two different approaches are possible. On the one hand, the principal axes are obtained for the total EFG and its different contributions are given with respect to these fixed axes ("collective axes"). On the other hand, the different contributions can also be defined relative to their own principal axes ("component axes"). The first procedure can be employed for the partitioning of the total V_{zz} into its contributions (such that the sum of the contributions yields the total). The corresponding results for the Y and D atoms in the different model structures are displayed in Tables IV and V, respectively, and will be discussed below. The second procedure is advantageous if the principal

TABLE III. Comparison of calculated EFG's for the structure models I, II, III, and IV with experimental results. The V_{zz} values are in units of 10^{20} V/m² and the lattice parameters in Å. The experimental results for D are from Ref. 18 and for ^{181}Ta at the Y position from Ref. 50.

Structure model		Positional parameters	Lattice parameters	V_{zz}	η	
I/II	Y: $6f$	$x = 0.6628$	$a = 6.3408$	23.0	0.33	
	D(<i>T</i>): $12g$	$x = 0.3521$	$c = 6.6061$	-1.9	0.80	
		$y = 0.0303$				
		$z = 0.0918$				
D(<i>m</i> 1): $2a$			-5.6	0.0		
D(<i>m</i> 2): $4d$	$z = 0.1875$		-5.1	0.0		
III	Y: $6c$	$x = 0.6704$	$a = 6.3441$	22.7	0.54	
		$z = 0.2502$	$c = 6.6117$			
	D(1): $6c$	$x = 0.3026$		-2.3	0.50	
		$z = 0.0915$				
	D(2): $6c$	$x = 0.3556$		1.7	0.62	
		$z = 0.4077$				
IV	Y: $6c$	$x = 0.6713$	$a = 6.3441$	23.3	0.51	
		$x = 0.6713$	$c = 6.6081$			
		$z = 0.2506$				
	D(1): $6c$	$x = -0.0183$		2.0	0.84	
		$y = -0.3667$				
		$z = 0.0922$				
	D(2): $6c$	$x = 0.3017$		-2.2	0.63	
		$y = -0.0042$				
		$z = -0.0911$				
	D(3): $2a$	$z = 0.1870$		-5.2	0.0	
D(4): $2b$	$z = 0.2788$		-5.3	0.0		
D(5): $2b$	$z = -0.1929$		-5.2	0.0		
Expt.	Y (^{181}Ta)			29.0	0.8	
	D			2.3	0.59 ± 0.05	
	D			5.6	0.0	

axes for the various contributions shall be related to particular atomic neighbors in the crystal lattice, and will therefore also be adopted here.

The Y EFG is almost completely determined by the sphere contribution, the main components of which are pp , dd , and semicore pp and are given in Table IV. Comparing the component axes for V_{xx}^{pp} and V_{yy}^{pp} with the bond directions

TABLE IV. Split of the Y EFG's for YD_3 into their main components, i.e., pp , dd , and semicore pp . The V_{zz} values are in units of 10^{20} V/m².

Structure model	V_{zz}	V_{zz}^{pp}	V_{zz}^{dd}	$V_{zz}^{pp(sc)}$
I/II	23.1	40.2	5.0	-22.1
III	22.7	40.4	5.0	-22.6
IV	23.3	40.5	4.9	-22.2

TABLE V. Split of the D EFG's for YD_3 into lattice and sphere contributions. For the latter its main component (sd) is given. The V_{zz} values are in units of 10^{20} V/m².

Model	D atom	V_{zz}	V_{zz}^{lat}	V_{zz}^{sph}	V_{zz}^{sd}
I/II	D(T)	-1.93	-2.80	0.87	0.71
	D($m1$)	-5.58	-8.27	2.69	2.20
	D($m2$)	-5.13	-7.38	2.25	1.94
III	D(1)	-2.29	-3.32	1.03	0.87
	D(2)	1.72	2.51	-0.79	-0.60
	D(3)	-5.22	-7.46	2.24	1.94
	D(4)	-5.25	-7.71	2.46	2.06
IV	D(1)	-2.00	-2.87	0.87	0.71
	D(2)	-2.22	-3.21	0.99	0.84
	D(3)	-5.19	-7.46	2.27	1.97
	D(4)	-5.32	-7.92	2.60	2.15
	D(5)	-5.23	-7.53	2.30	1.96

shows that in all structure models the values for V_{xx}^{pp} and V_{yy}^{pp} are negative and correspond to interactions of Y with neighboring Y atoms and with octahedral D atoms [designated by D($m1$) and D($m2$) for model I/II, by D(3) and D(4) for model III, and D(3) to D(5) for model IV in Tables II, III, and V]. These D atoms are at a distance of circa 2.14 Å from Y. For the tetrahedral D atoms (at a distance of roughly 2.26 Å) V_{zz}^{pp} are positive, and therefore indicate a weaker Y-D interaction.

The dd EFG components are mainly determined by the Y-Y interactions. They are smaller than the pp components by roughly one order of magnitude. This is due to the slower increase of the d electron density near the nucleus compared to the p density, as shown by Blaha *et al.*⁴⁴

The semicore pp components for Y do not depend directly on the atomic neighbors about the Y atom, but result from polarizing effects of the valence electrons on the semicore $4p$ states. This leads to opposite signs for the valence and semicore EFG components. In this way an energetically and electrostatically favorable arrangement is reached.

Finally, the D EFG's are discussed. The results are very similar for the different structure models, but striking differences exist between the tetrahedral and octahedral D atoms. Larger negative V_{zz} values belong to the octahedral D atoms with their Y neighbors at circa 2.14 Å, and smaller negative or positive values to the tetrahedral D atoms whose nearest Y neighbors are about 2.27 Å apart. Table V shows that in contrast to the Y atoms with their negligible lattice contributions, for the D atoms the lattice contributions are much larger than the sphere contributions. Here the sphere contributions are dominated by the sd components in contrast to the Y EFG's where pp and, to a lesser extent, dd are the main components.

V. OPTICAL PROPERTIES

Comparison of electric-field gradients as calculated for several suggested structures with those obtained from experi-

ments provided indication for the $P6_3cm$ symmetry (structure type III) as being the most promising candidate. Since the optical appearance of YH_3 and its dramatic change with decreased hydrogen contents is the outstanding property that attracted so much attention, it is desirable to investigate the optical properties of structure III in detail.

Among the structural models considered here, electronic band-structure calculations have so far been published only for the $P\bar{3}c1$ symmetry (structures I and II). Studies based on standard density-functional theory did not confirm the semiconducting state, but rather yielded a band overlap of about 1.0–1.3 eV (pseudopotential methods),^{9,45,46} and of about 0.7–0.9 eV (all-electron methods) (Refs. 47 and 53) around the Γ point. Optical transmission and reflection experiments, however, clearly indicate an optical band gap in the range of 2.3–2.8 eV.^{1,54,55} The fundamental band gap was given as 1.8 eV in the original experimental study on switchable mirror systems.¹ The most recent reflectance, transmittance, and ellipsometry measurements specify an optical band gap of 2.63 eV, and provide indications of a fundamental band gap at 1–1.8 eV lower energy.⁵⁶ The discrepancy between experiment and theory with regard to the band gap gave rise to different speculations. Although it is well known that standard density-functional theory usually tends to underestimate the size of band gaps, the discrepancy of 3–4 eV is exceptionally large. Errors of this magnitude have been observed in transition-metal oxides, where strongly correlated d electrons are poorly represented by standard DFT. It was thus suggested that similar strong correlation effects of electrons on hydrogen sites may be responsible for the large band gap.^{57–59} A fairly different explanation for the large band-gap error argues with a strong electron-phonon coupling effect revealed by first-principles calculations.¹² Symmetry-breaking displacements of hydrogen atoms were found to reduce the total energy of the $P\bar{3}c1$ structure. The resulting structure model has a $P6_3$ symmetry (structure type IV) and exhibits a small band gap of 0.8 eV even within a standard LDA description. The remaining discrepancy to the measured optical band gap can thus be considered clearly within the usual magnitude of the failure of standard DFT. A further attempt to understand the optical properties of YH_3 was pursued by *ab initio* quasiparticle band-structure calculations of the $P\bar{3}c1$,^{45,46} LaF_3 ,^{45,46,60} and the BiF_3 (Ref. 60) structural models within the GW approximation. This computational approach overcomes the deficiencies of DFT, allowing band-gap prediction with an accuracy of a few tenths of an eV. For the $P\bar{3}c1$ structure a fundamental band gap of only 1.0 eV at Γ is calculated. It is, however, argued that the fundamental band gap arises from backfolding of the conduction band at K of the LaF_3 to Γ of the $P\bar{3}c1$ structure and, therefore, corresponds to a forbidden excitation that cannot be observed in the optical spectra. The first visible transition may involve the second lowest conduction state at Γ , yielding an optical band gap of 2.8 eV as observed experimentally.

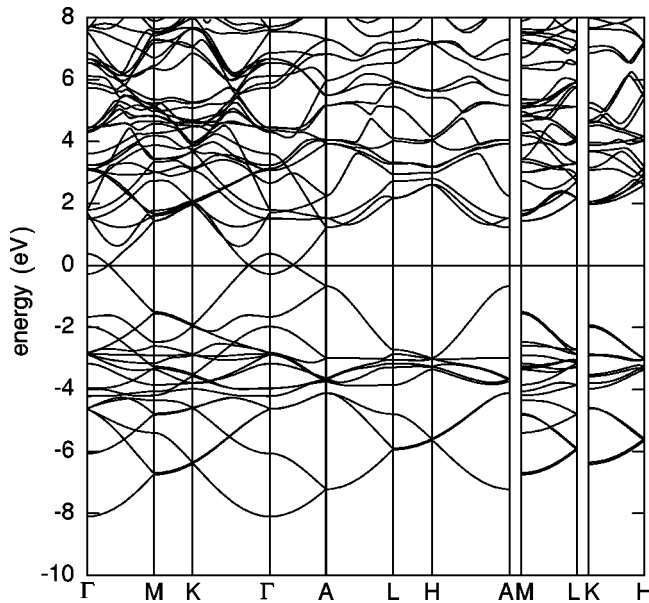


FIG. 1. LDA band structure for YH_3 (structure type III, space group $P6_3cm$).

Whereas in all these contributions optical properties of YH_3 were theoretically studied assuming the $P\bar{3}c1$ or simpler structures, the present work focuses on the $P6_3cm$ structure that has been identified as the most promising candidate according to our EFG results. The band structure of YH_3 within the LDA to standard DFT is given in Fig. 1. Within this approach we find YH_3 to be a semimetal with a single band overlap of about 0.7 eV at the Γ point. Qualitatively, this result is in accordance with other standard DFT calculations for the $P\bar{3}c1$ structural model. In order to overcome the well-known inadequacy of standard DFT in representing excitation energies and band gaps of semiconductors and insulators, we adopted the screened nonlocal exchange approach.^{19,20} A brief description of the approach and the computational details are given in Sec. II A. The sX-LDA band structure is shown in Fig. 2. The band overlap at Γ has disappeared, and a direct fundamental band gap of about 1.85 eV has opened up in accordance with the value of 1.8 eV reported in Ref. 1. The second conduction band is located about 2.9 eV above the valence band edge at the Γ point and may be interpreted as responsible for the experimentally observed optical band gap (absorption edge).

In comparing the sX-LDA band structure of the $P6_3cm$ structure model with the GW band structure for the $P\bar{3}c1$ symmetry from Ref. 45,46, the most obvious difference is the much smaller fundamental band gap of 1.0 eV provided by the GW result. Part of the difference is already contained in the larger band overlap, the more important part, however, is a smaller band shift for the conduction band edge due to the GW approach. Nevertheless, the second conduction state at Γ is equally located 2.8–2.9 eV above the valence-band edge. It seems, however, that the origin and characteristics of this band might be entirely different. Currently, a clear separation of methodological and structural effects is not possible and further investigations are required.

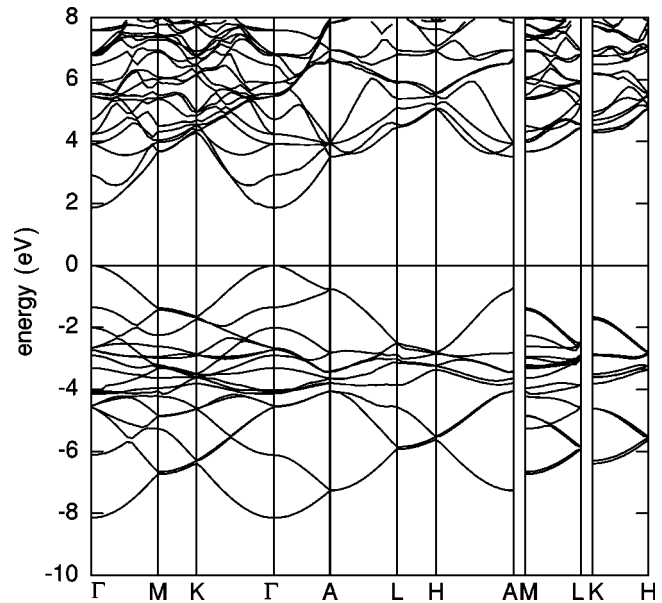


FIG. 2. sX-LDA band structure for YH_3 (structure type III, space group $P6_3cm$).

For a unique identification of optically active transitions it is necessary to calculate optical matrix elements. We have systematically calculated optical matrix elements for transitions at and in the vicinity of the Γ point within the sX-LDA approach. As a matter of fact, the matrix elements of transitions corresponding to the fundamental band gap as well as those for the assumed optical band gap are almost vanishing. The same is true for all other investigated transitions in the energy range below 5 eV. Consequently, we cannot provide clear evidence of the transitions involved in absorption processes. It is noted, however, that the situation might change completely once symmetry lowering effects caused by off-stoichiometry or impurities are taken into account.

VI. CONCLUSIONS

An unambiguous structure assignment for the semiconducting YH_3 phase is still an open issue in understanding the physics of switchable mirror systems. Directly approaching this open question, structural optimizations and total-energy calculations based on the density-functional theory are reported. Unfortunately, the obtained energy differences are too small to provide a decisive answer. Based on optimized model structures, EFG's of the candidate structures were calculated and compared with results obtained experimentally from nuclear magnetic resonance studies. The deuterium EFG's of the $P6_3cm$ structure show the best agreement. Furthermore, calculated yttrium EFG's are found to be rather similar for the $P6_3cm$ and $P6_3$ structures, but different from those found for the $P\bar{3}c1$ structure. Unfortunately, Y EFG's cannot be measured directly, and suitable substitutions need to be identified. PAC experiments for a Ta substitution provide EFG's quite close to those calculated for the $P6_3cm$

and $P6_3$ structures. However, the validity of the substitution might be questionable. Further experimental EFG studies aiming at suitably substituted Y nuclei are required. Finally, the band structure and optical properties of the $P6_3cm$ structural model were investigated, and found to be in accordance with available transmission and reflection studies.

ACKNOWLEDGMENTS

The authors are grateful to O. J. Żogał and P. Vajda for stimulating and fruitful discussions and to the Hochschuljubiläumsstiftung der Stadt Wien (Project H-44/99) for financial support.

- ¹J. N. Huiberts, R. Griessen, J. H. Rector, R. J. Wijngaarden, J. P. Dekker, D. G. de Groot, and N. J. Koeman, *Nature* (London) **380**, 231 (1996).
- ²P. Vajda, in *Handbook on the Physics and Chemistry of Rare Earths*, edited by K. A. Gschneidner, Jr. and L. Eyring (Elsevier, Amsterdam, 1995), Vol. 20, p. 207.
- ³W. M. Mueller, in *Metal Hydrides*, edited by W. M. Mueller, J. P. Blackledge, and G. G. Libowitz (Academic, New York, 1968), p. 384.
- ⁴G. G. Libowitz, *Ber. Bunsenges. Phys. Chem.* **76**, 837 (1972).
- ⁵G. G. Libowitz and A. J. Maeland, in *Handbook on the Physics and Chemistry of Rare Earths*, edited by K. A. Gschneidner, Jr. and L. Eyring (North-Holland, Amsterdam, 1979), Vol. 3, p. 299.
- ⁶N. F. Miron, V. I. Shcherbak, V. N. Bykov, and V. A. Levdivik, *Sov. Phys. Crystallogr.* **17**, 404 (1972)].
- ⁷A. Pebler and W. E. Wallace, *J. Phys. Chem.* **66**, 148 (1962).
- ⁸T. J. Udovic, Q. Huang, and J. J. Rush, *J. Phys. Chem. Solids* **57**, 423 (1996).
- ⁹Y. Wang and M. Y. Chou, *Phys. Rev. B* **51**, 7500 (1995).
- ¹⁰T. J. Udovic, Q. Huang, and J. J. Rush, in *Hydrogen in Semiconductors and Metals*, edited by N. N. Nickel, W. B. Jackson, R. C. Bowman, and R. G. Leisure, MRS Symposia Proceedings No. 513 (Materials Research Society, Pittsburgh, 1998), p. 197.
- ¹¹T. J. Udovic, Q. Huang, R. W. Erwin, B. Hjörvarsson, and R. C. C. Ward, *Phys. Rev. B* **61**, 12 701 (2000).
- ¹²P. J. Kelly, J. P. Dekker, and R. Stumpf, *Phys. Rev. Lett.* **78**, 1315 (1997).
- ¹³T. J. Udovic, Q. Huang, and J. J. Rush, *Phys. Rev. Lett.* **79**, 2920 (1997).
- ¹⁴P. J. Kelly, J. P. Dekker, and R. Stumpf, *Phys. Rev. Lett.* **79**, 2921 (1997).
- ¹⁵P. van Gelderen, P. J. Kelly, and G. Brocks, *Phys. Rev. B* **63**, 100301 (2001).
- ¹⁶H. Kierey, M. Rode, A. Jacob, A. Borgschulte, and J. Schoenes, *Phys. Rev. B* **63**, 134109 (2001).
- ¹⁷P. Herzig, W. Wolf, and O. J. Żogał, *Phys. Rev. B* **62**, 7098 (2000).
- ¹⁸O. J. Żogał, W. Wolf, P. Herzig, A. H. Vuorimäki, E. E. Ylinen, and P. Vajda, *Phys. Rev. B* **64**, 214110 (2001).
- ¹⁹D. M. Bylander and L. Kleinmann, *Phys. Rev. B* **41**, 7868 (1990).
- ²⁰A. Seidl, A. Görling, P. Vogl, J. A. Majewski, and M. Levy, *Phys. Rev. B* **53**, 3764 (1996).
- ²¹<http://cms.mpi.univie.ac.at/vasp/>;
<http://www.materialsdesign.com/Pages/VASP.htm>
- ²²G. Kresse and J. Furthmüller, *Phys. Rev. B* **54**, 11 169 (1996).
- ²³G. Kresse and J. Furthmüller, *Comput. Mater. Sci.* **6**, 15 (1996).
- ²⁴P. Hohenberg and W. Kohn, *Phys. Rev.* **136**, B864 (1964).
- ²⁵W. Kohn and L. J. Sham, *Phys. Rev.* **140**, A1133 (1965).
- ²⁶P. E. Blöchl, *Phys. Rev. B* **50**, 17 953 (1994).
- ²⁷G. Kresse and D. Joubert, *Phys. Rev. B* **59**, 1758 (1998).
- ²⁸D. Vanderbilt, *Phys. Rev. B* **41**, 7892 (1990).
- ²⁹J. P. Perdew and A. Zunger, *Phys. Rev. B* **23**, 5048 (1981).
- ³⁰J. P. Perdew, J. A. Chevary, S. H. Vosko, K. A. Jackson, M. R. Pederson, D. J. Singh, and C. Fiolhais, *Phys. Rev. B* **46**, 6671 (1992).
- ³¹H. J. Monkhorst and J. D. Pack, *Phys. Rev. B* **13**, 5188 (1976).
- ³²O. Jepsen and O. K. Andersen, *Solid State Commun.* **9**, 1763 (1971).
- ³³G. Lehmann and M. Taut, *Phys. Status Solidi B* **54**, 469 (1972).
- ³⁴P. E. Blöchl, O. Jepsen, and O. K. Andersen, *Phys. Rev. B* **49**, 16 223 (1994).
- ³⁵O. K. Andersen, *Phys. Rev. B* **12**, 3060 (1975).
- ³⁶D. D. Koelling and G. O. Arbman, *J. Phys. F: Met. Phys.* **5**, 2041 (1975).
- ³⁷E. Wimmer, H. Krakauer, M. Weinert, and A. J. Freeman, *Phys. Rev. B* **24**, 864 (1981).
- ³⁸H. J. F. Jansen and A. J. Freeman, *Phys. Rev. B* **30**, 561 (1984).
- ³⁹B. I. Min, T. Oguchi, H. J. F. Jansen, and A. J. Freeman, *J. Magn. Magn. Mater.* **54-57**, 1091 (1986).
- ⁴⁰L. Hedin and B. I. Lundqvist, *J. Phys. C* **4**, 2064 (1971).
- ⁴¹L. Hedin and S. Lundqvist, *J. Phys. (Paris), Colloq.* **33**, C3-73 (1972).
- ⁴²P. Herzig, *Theor. Chim. Acta* **67**, 323 (1985).
- ⁴³P. Blaha, K. Schwarz, and P. Herzig, *Phys. Rev. Lett.* **54**, 1192 (1985).
- ⁴⁴P. Blaha, K. Schwarz, and P. H. Dederichs, *Phys. Rev. B* **37**, 2792 (1988).
- ⁴⁵P. van Gelderen, P. A. Bobbert, P. J. Kelly, and G. Brocks, *Phys. Rev. Lett.* **85**, 2989 (2000).
- ⁴⁶P. van Gelderen, P. A. Bobbert, P. J. Kelly, G. Brocks, and R. Tolboom, *Phys. Rev. B* **66**, 075104 (2002).
- ⁴⁷J. P. Dekker, J. van Ek, A. Lodder, and J. N. Huiberts, *J. Phys.: Condens. Matter* **5**, 4805 (1993).
- ⁴⁸W. Wolf, E. Wimmer, S. Massidda, M. Posternak, and C. B. Geller, *Bull. Am. Phys. Soc.* **43**, 797 (1998).
- ⁴⁹C. B. Geller, W. Wolf, S. Picozzi, A. Continenza, R. Asahi, W. Mannstadt, A. J. Freeman, and E. Wimmer, *Appl. Phys. Lett.* **79**, 368 (2001).
- ⁵⁰M. Forker, U. Hütten, and M. Lieder, *Phys. Rev. B* **49**, 8556 (1994).
- ⁵¹J. J. Balbach, M. S. Conradi, M. M. Hoffmann, T. J. Udovic, and N. L. Adolphi, *Phys. Rev. B* **58**, 14 823 (1998).
- ⁵²A. H. Vuorimäki, E. E. Ylinen, B. Nowak, and O. J. Żogał, *Solid State Commun.* **122**, 469 (2002).
- ⁵³R. Ahuja, B. Johansson, J. M. Wills, and O. Eriksson, *Appl. Phys. Lett.* **71**, 3498 (1997).

- ⁵⁴A. T. M. van Gogh, E. S. Kooij, and R. Griessen, *Phys. Rev. Lett.* **83**, 4614 (1999).
- ⁵⁵R. Griessen, J. N. Huiberts, M. Kremers, A. T. M. van Gogh, N. J. Koeman, J. P. Dekker, and P. H. L. Notten, *J. Alloys Compd.* **253-254**, 44 (1997).
- ⁵⁶A. T. M. van Gogh, D. G. Nagengast, E. S. Kooij, N. J. Koeman, J. H. Rector, R. Griessen, C. F. J. Flipse, and R. J. J. G. A. M. Smeets, *Phys. Rev. B* **63**, 195105 (2001).
- ⁵⁷K. K. Ng, F. C. Zhang, V. I. Anisimov, and T. M. Rice, *Phys. Rev. Lett.* **78**, 1311 (1997).
- ⁵⁸K. K. Ng, F. C. Zhang, V. I. Anisimov, and T. M. Rice, *Phys. Rev. B* **59**, 5398 (1999).
- ⁵⁹R. Eder, H. F. Pen, and G. A. Sawatzky, *Phys. Rev. B* **56**, 10 115 (1997).
- ⁶⁰T. Miyake, F. Aryasetiawan, H. Kino, and K. Terakura, *Phys. Rev. B* **61**, 16 491 (2000).
- ⁶¹Very recently for the same sample used by Żogał *et al.* (Ref. 18) also ^{89}Y NMR spectra, spin-lattice relaxation rates $1/T_1$, and magnetic susceptibilities over a temperature range of 1.8–300 K were published (Ref. 52).